Journal of Applied Polymer Science

Freestanding fiber mats of zeolitic imidazolate framework 7 via one-step, scalable electrospinning

Seongpil An,[1] Ji Sun Lee,[2,3] Bhavana N. Joshi,[1] Hong Seok Jo,[1] Kirill Titov,[4] Jong-San Chang,[2,5] Chul-Ho Jun,[3] Salem S. Al-Deyab,[6] Young Kyu Hwang,[2] Jin-Chong Tan,[4] Sam S. Yoon[1]

[1]School of Mechanical Engineering, Korea University, Seoul 02841, Republic of Korea
[2]Research Group for Nanocatalysts, Korea Research Institute of Chemical Technology, Daejeon 34114, Republic of Korea
[3]Deparment of Chemistry, Center for Bioactive Molecular Hybrids, Yonsei University, Seoul 03722, Republic of Korea
[4]Department of Engineering Science, University of Oxford, Parks Road Oxford OX1 3PJ, United Kingdom
[5]Department of Chemistry, Sungkyunkwan University, Suwon 16419, Republic of Korea
[6]Department of Chemistry, College of Science, King Saud University, Riyadh 11451, Saudi Arabia
S. An and J. S. Lee contributed equally to this article.
Correspondence to: Y. K. Hwang (E-mail: ykhwang@krict.re.kr), J. C. Tan (E-mail: jin-chong.tan@eng.ox.ac.uk), and S. S. Yoon (E-mail: skyoon@korea.ac.kr)

ABSTRACT: We demonstrated the fabrication of freestanding zeolitic imidazolate framework 7 (ZIF-7) nanofiber (NF) mats by means of one-step, scalable electrospinning. The formation of ZIF-7 nanoparticles embedded in polymer fibers was unambiguously pinpointed via X-ray diffraction, transmission electron microscopy, and adsorption studies. The NF mats exhibited excellent characteristics, with an average diameter of 245 nm, in the adsorption and desorption of carbon dioxide (CO_2); this makes them attractive candidates for gas separation and other selective filtration applications. This excellent property of the ZIF-7 mats was explained by the gate-opening phenomenon of ZIF-7, which yielded a stepwise increase in the overall CO_2 uptake capacity. The mechanical strength of the NF mats was also obtained via large-strain uniaxial tensile deformation, which enabled preliminary assessment of the mat's suitability for textiles and membranes in targeting separation and filtration applications with large-area permeability. © 2016 Wiley Periodicals, Inc. J. Appl. Polym. Sci. **2016**, *133*, 43788.

KEYWORDS: electrospinning; fibers; surfaces and interfaces; synthesis and processing

Received 16 February 2016; accepted 12 April 2016
DOI: 10.1002/app.43788

INTRODUCTION

Advancements in modern industry and society have increased fossil fuel consumption dramatically; this, in turn, has increased greenhouse gas emissions.[1] According to the prediction of the Intergovernmental Panel on Climate Change,[2] the rise in the carbon dioxide (CO_2) concentration in environment will increase global temperatures by 1.9 °C. Thus, the need to develop new technology capable of capturing CO_2 has become an urgent issue. Various techniques have been developed for anthropogenic CO_2 capture; these include amine–solvent scrubbing, cryogenic distillation, solid sorbents, and more.[3,4] In this context, metal–organic frameworks (MOFs) have recently generated considerable research interest because of their well-ordered pore structure, high surface area, flexible dynamic behavior in response to guest molecules, and designable functionalization of channel surfaces. This unique combination of material properties provides exciting potential for CO_2 capture applications.[5] These qualities of MOFs also suggest various other applications, such as gas storage and purification,[6] catalysis,[7] molecular recognition, and drug delivery.[8]

Zeolitic imidazolate frameworks (ZIFs) are a topical family of MOF materials constructed by the coordination of imidazole-based organic linkers and zinc tetrahedra (ZnN_4) to produce a myriad of porous frameworks that mimic the topology of zeolites (aluminosilicates).[9] ZIFs are highly versatile and potentially useful for various applications because of their good chemical stability[9] and tunable pore structures, which confer a wide range of mechanical properties[10] and intriguing framework dynamics;[11] thereby, they have attracted considerable interest in the fields of gas separation, gas sensors,[12,13] catalysis,[14,15] and

Additional Supporting Information may be found in the online version of this article

biotechnology.[16] Recent studies have established that ZIFs (including ZIF-7, ZIF-8, and ZIF-68) exhibit a relatively high thermal stability of up to 673 K.[17] The pore apertures (windows) of ZIF-7 and ZIF-8 estimated by crystallographic data are about 0.3 and 0.34 nm, respectively.[18] These values correspond to the molecular sizes of H_2O (0.265 nm), H_2 (0.289 nm), CO_2 (0.305 nm), and N_2 (0.364 nm).[19] As in the case of zeolites, the kinetic separation of C_2 (ethane/ethylene) and C_3(propane/propylene) was successfully demonstrated with small-sized windows of ZIF-7 and ZIF-8.[20] It is worth noting that ZIF-7 has a high window flexibility toward a pressure stimulus; this results in improved sorption characteristics and affords H_2 and CO_2 separations;[21] likewise, this flexibility opens it up for new applications in gas separation, such as in the accommodation of N_2O and C_2–C_4 adsorption.[6]

Although ZIF has numerous potential applications, its industrial use requires shaping or joining processes to create modules suitable for large-scale deployments. It is generally accepted that nanocomposite structures of MOFs are vital for MOF applications for two important reasons: nanocomposites composed of MOFs and polymer nanofibers (NFs) can be easily separated from heterogeneous solutions of adsorbent and adsorbate, and also, shaped MOFs can be used to realize catalytic and separation applications.[22] For that purpose, many experiments have been performed to make MOF nanocomposites between MOFs and MOFs, MOFs and inorganic materials, and MOFs and organic materials, including MOFs and polymers.[23] Among them, MOF–polymer NFs, such as ZIF-8/polyvinylpyrrolidone[24] and copper benzene-1,3,5-tricarboxylate/polymers,[25] have attracted much attention in the separation and purification of gas and liquid mixtures.[26] The use of NFs from different materials have been proven to be beneficial in various applications, such as filtration, controlled drug release, anode materials, sensors, and catalysis.[22] To increase the efficiency of filtration/gas separation, porous fibers present clear advantages against a dense (monolithic) bulk material. Despite the preceding NF studies on MOFs,[24,27–30] studies on ZIF-8 have been limited. Although ZIF-7 [Zn(benzimidazolate)$_2$] is akin to ZIF-8 [Zn(2-methylimidazolate)$_2$] in terms of its sodalite topology,[9] as mentioned previously, it has a relatively smaller pore aperture (window size); this makes it particularly suitable for CO_2 capture compared to other gases. ZIF-7 was first discovered by Huang *et al.*[31] in 2003. Various synthesis procedures have been reported for the fabrication of ZIF films and membranes; these can be classified into two categories: *in situ* growth and secondary (seeded) growth.[22] The secondary growth method requires a seeding step in addition to the solvothermal growth step. The increased number of preparation steps makes this process very complex and, thus, lowers its reproducibility.[15,32,33]

Herein, we report on the fabrication of ZIF-7/polyacrylonitrile (PAN) nanocomposite fibers with the scalable method, in which ZIF-7 nanoparticles (NPs) were formed during the reaction and were aligned directly with the fibers during the electrospinning process. Significantly, this synthesis route is a one-step process, and it does not require cumbersome solvothermal treatments. In this study, for the first time, we produced ZIF-7/PAN nanocomposite fibers supporting a well-ordered microporous ZIF structure, and this could open up new possibilities in CO_2 gas capture and separation. The mechanical properties of the MOF fibers are also very important for various technical applications. For example, the intrinsic porosity of ZIFs should be maintained during sorption/desorption cycles, whereas at the macroscale, the fiber nanocomposite as a whole must be mechanically resilient to withstand stresses and strain arising from service.[34] Thus, the characterization of the core mechanical properties of the PAN and ZIF-7/PAN NFs was also carried out in this study.

EXPERIMENTAL

Starting Materials

Zinc nitrate hexahydrate [$Zn(NO_3)_2{\cdot}6H_2O$; 98%, Sigma-Aldrich] and benzimidazole ($C_7H_6N_2$; 98%, Sigma-Aldrich) were used as the metal and ligand sources, respectively. *N,N*-Dimethylformamide (DMF; 99.8%, Sigma-Aldrich) and methanol (99.8%, Samchun Chemical) were used as solvents without further purification. PAN (weight-average molecular weight = 150 kDa) was used as a solute for the electrospinning solution.

Synthesis of the ZIF-7/PAN NFs

Figure 1(a) shows the synthesis process of the ZIF-7/PAN solution. Solutions of 8 wt % $Zn(NO_3)_2{\cdot}6H_2O$ and 4 wt % $C_7H_6N_2$ in DMF were mixed, and immediately, a certain amount of PAN powder was added to the mixed solution to make a 6 wt % ZIF-7/PAN precursor. Next, the precursor was stirred at 50 °C for 3 days to crystalize ZIF-7, and thereby, ZIF-7-containing NFs could be deposited without posttreatments. Specifically, with respect to the case of CO_2 adsorption, different stirring temperatures of 50, 100, and 150 °C were used for the preparation to investigate whether the synthesis temperature affected the material performance.

Uniform ZIF-7/PAN NFs were electrospun on a stainless steel substrate at 36% humidity and under room temperature, as shown in Figure 1(b). The flow rate of 150 μL/h was supplied by a syringe pump (Legato 100, KD Scientific, Inc.), and a voltage of 7 kV was given by a high-voltage power supply (EP20P2, Glassman High Voltage, Inc.). The nozzle used had 0.84 and 1.27 mm inner and outer diameters, respectively, and the distance between the nozzle and substrates was fixed at 10 cm.

Synthesis of the ZIF-7 NPs

ZIF-7 NPs were prepared by a conventional solvothermal method. Typically, a solution of $C_7H_6N_2$ (810 mg, 6.86 mmol) and a solution of $Zn(NO_3)_2{\cdot}6H_2O$ (1530 mg, 5.14 mmol) in 40 mL of DMF were mixed in a Teflon vessel and then reacted at 50 °C for 3 days under the same conditions to resemble the synthesis of the NFs. After the solvothermal synthesis, the products were purified by centrifugation and then washed with methanol three times to remove any unreacted reactants. Finally, the products were dried overnight below 100 °C in an air atmosphere. The concentration of the reactant was similar to that used for the preparation of the electrospinning solution.

Material Characterization

To characterize and analyze the ZIF-7/PAN NFs produced, scanning electron microscopy (SEM, S-5000, Hitachi, Ltd.), transmission electron microscopy (TEM; JEM-2100F, JEOL, Inc.), energy-dispersive X-ray spectroscopy (EDX) with TEM, X-ray

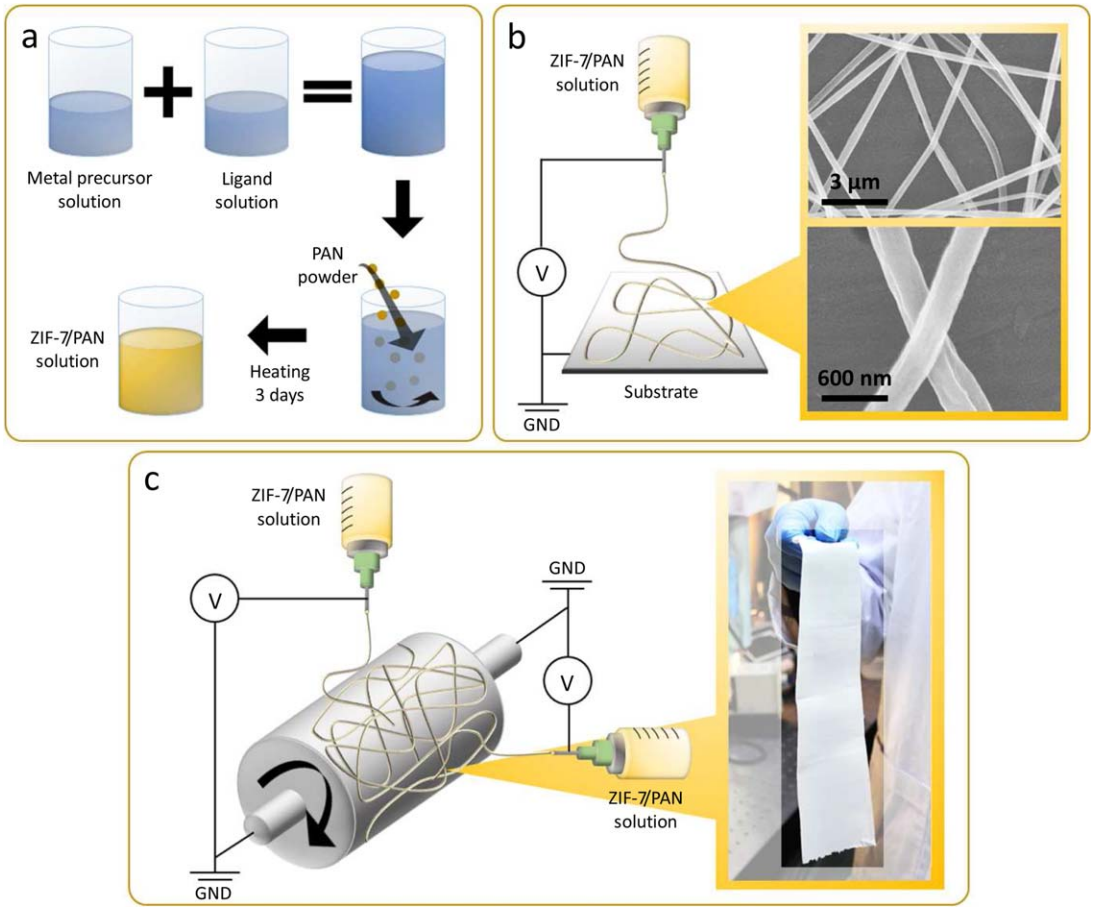

Figure 1. Schematics of (a) the synthesis process of the ZIF-7/PAN solution and the experimental setups used for (b) single-nozzle electrospinning, including SEM images of the resulting fibers, and (c) multinozzle electrospinning with a drum collector. *V* voltage supply. *GND* ground electrode. [Color figure can be viewed in the online issue, which is available at wileyonlinelibrary.com.]

diffraction (XRD; SmartLab, Rigaku), thermogravimetric analysis (TGA; N-1000, SCINCO M&T), CO_2 adsorption (Micromeritics), and mechanical testing (Instron tensometer) were used. The XRD patterns were recorded on an X-ray diffractometer with Cu Kα ($\lambda = 1.5406$ Å) radiation. The ZIF-7/PAN NFs samples used in SEM analysis were coated with a thin layer of platinum by an ion sputter coater before imaging. A thermogravimetric analyzer was used to determine the TGA curves with the sample held in a platinum pan under air atmosphere at a heating rate of 5 °C/min. Moreover, the CO_2 adsorption and desorption isotherms were used to determine the porosity of the ZIF-7/PAN NFs with a volumetric adsorption apparatus (Tristar 3020, Micromeritics). A standard volumetric technique was applied to obtain the sorption data of small gas molecules in the pressure range from 5 to 760 Torr, if not otherwise specified. The sample was dehydrated at 150 °C for 3 h under a high vacuum ($<10^{-6}$ Torr) before we started the adsorption studies. Even though the pores of ZIF-7 were flexible (because of gate-opening phenomenon), which enabled larger molecules to enter,[11] the pore size of ZIF-7 is generally smaller than the kinetic diameter of N_2, as mentioned previously.[35] Therefore, CO_2 was selected to study the sorption characteristics of the ZIF-7 crystals. To confirm the permanent porosity of the ZIF-7/PAN NFs, we examined the CO_2 adsorption–desorption isotherms at 196 K (−77 °C; shown later in Figure 6). The sample cell was loaded with about 0.18 g of NF mat. The test pieces for mechanical studies were 5 mm (width) × 20 mm (gauge length). Thickness of the specimens was between 30 to 80 μm, each of which individually determined using a digital micrometer. The Instron tensometer was equipped with a 100 N load cell, operating at a constant displacement rate of 1 mm/min.

RESULTS AND DISCUSSION

Figure 1(b) shows representative SEM images of the NFs deposited after 30 s of electrospinning. The diameter of the fibers was estimated by the averaging of the individual values of 200 fibers; this amounted to an average fiber diameter of 245 nm with a standard deviation of 43 nm. There was scope to tune the average diameter of the NFs through variation in the polymer concentration. An image of a mat of ZIF-7/PAN NFs is shown in Figure 1(c). The mat appeared to be of milky color because of the submicrometer fiber size. As shown in Figure 1(c), we demonstrated that the macroscopic nonwoven mat could be obtained at a reasonably large scale. Thus, the composite fibers could be scaled up like MOF textiles; this would simultaneously

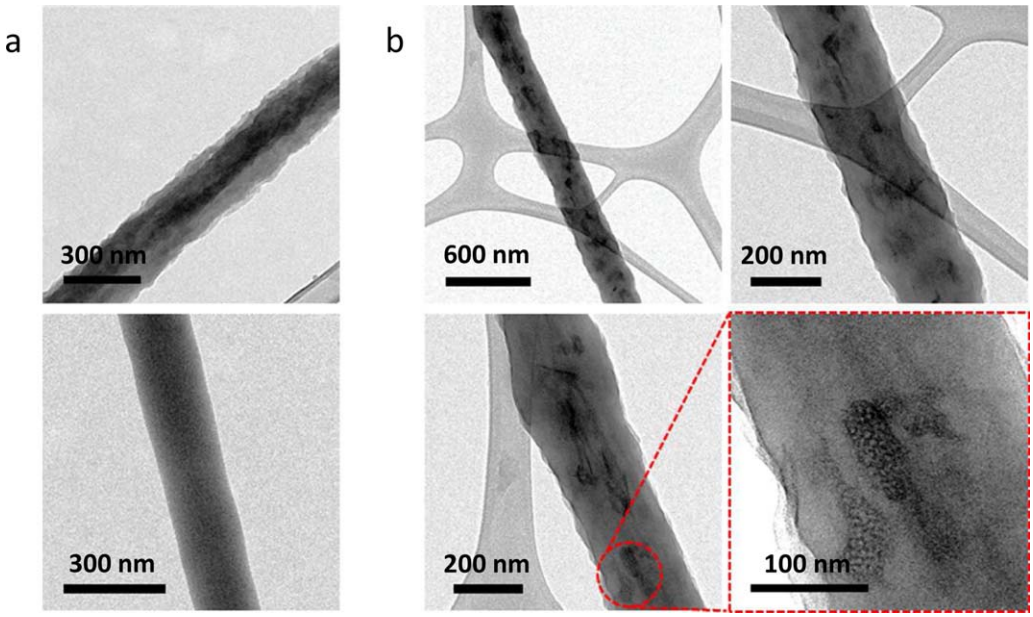

Figure 2. TEM images of (a) a single ZIF-7/PAN NF (top) and PAN NF (bottom) and (b) ZIF-7/PAN composite NFs at various magnifications. [Color figure can be viewed in the online issue, which is available at wileyonlinelibrary.com.]

combine the unique properties of both polymeric fibers and MOFs. The NFs obtained in the form of nonwoven mats were subsequently used for detailed characterizations, as described later.

TEM studies revealed the homogeneous distribution of the ZIF-7 NPs embedded in a polymeric fiber, as shown in Figure 2(a, top). In contrast, the neat PAN NFs in Figure 2(a, bottom) retained a smooth and uniform surface with an average fiber diameter of 200–300 nm. The magnified TEM images of the composite ZIF-7/PAN NFs [Figure 2(b)] clearly showed that the fiber surface became more corrugated (increased roughness) because of the loading of ZIF-7 in the PAN NF; we also noted that the distribution of ZIF-7 was homogeneous to a large extent. The elemental analysis of the ZIF-7/PAN NFs carried out by TEM–EDX is presented in Figure 3 and clearly shows that the higher concentration of carbon came from the polymer PAN (matrix phase). Zn atoms detected via elemental mapping could be ascribed to the ZIF-7 NPs embedded and coated all over the fiber. The presence of other elements, particularly nitrogen (originating from PAN and ZIF-7) and oxygen (originating from water absorbed on the NFs), was also observed in some small percentages.

Figure 4(a) shows the XRD patterns of the pristine ZIF-7 NPs, PAN NFs, and ZIF-7/PAN NFs. The ZIF-7 pattern exhibited the characteristic ZIF-7 peaks at 2θs of 7.15, 7.65, 10.5, 12.09, 13.03, 15.37, 18.64, 19.60, 21.1, and 23°.[36] The broad and dominant peak of PAN around 17° corresponded to the orthorhombic (110) orientation in the case of PAN NFs.[37] PAN and ZIF-7 peaks were clearly observed for the composite fibers, and this confirmed the successful spinning of the ZIF-7/PAN NFs. Additionally, XRD patterns of other synthesis temperatures of 100 and 150 °C cases have been considered, and the data suggest that the overall crystallization of ZIF-7 in the NFs increased as the synthesis temperature increased, as depicted in Figure 4(a). This synthesis temperature effect was also demonstrated in the CO_2 adsorption results. Figure 4(b) shows the effect of three different annealing temperatures on the ZIF-7/PAN NF mat (which was synthesized at 50 °C). The sample was heated from room temperature to 200 or 400 °C for 1 h at a heating rate of 5 °C/min in an argon atmosphere. The figure clearly shows that ZIF-7 retained its structure up to 200 °C; however, it degraded at 400 °C (thermal amorphization).[38] At 400 °C, diffraction peaks corresponding to the ZIF-7 structure were no longer discernible; the peak generated at 35° (belonging to ZnO as per

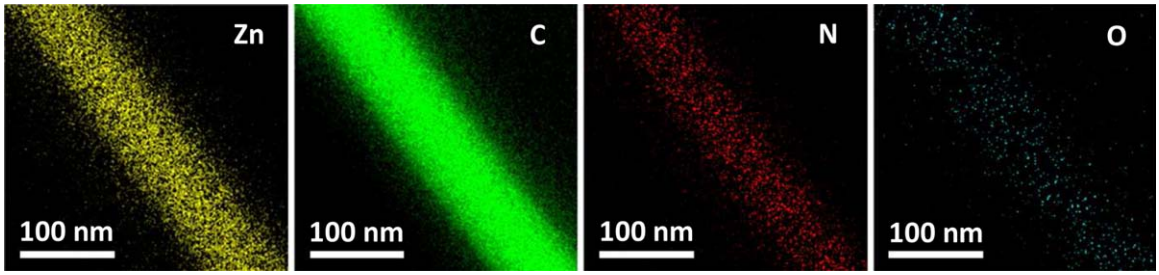

Figure 3. TEM–EDX elemental mapping of the ZIF-7/PAN NFs. [Color figure can be viewed in the online issue, which is available at wileyonlinelibrary.com.]

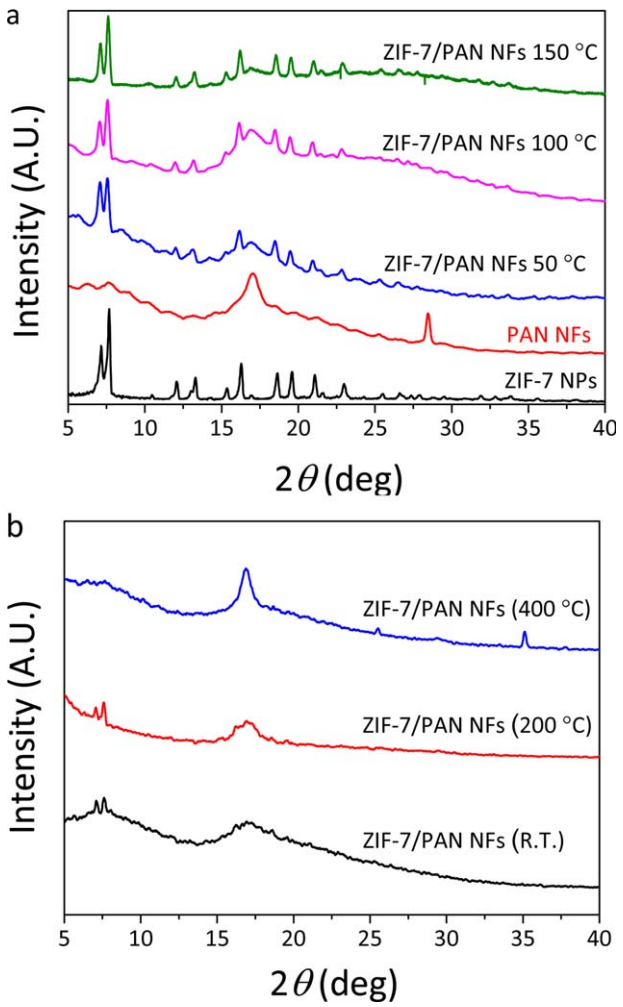

Figure 4. XRD patterns of (a) ZIF-7/PAN at synthesis temperatures of 50, 100, and 150 °C, PAN NFs, and ZIF-7 NPs and (b) ZIF-7/PAN NFs annealed at different temperatures. [Color figure can be viewed in the online issue, which is available at wileyonlinelibrary.com.]

JCPDS card 36-1451) confirmed that ZIF-7 was converted to ZnO. To better verify the conversion, XRD analyses of the ZIF-7 NPs (without PAN) at different annealing temperatures were conducted (Supporting Information, Figure S2), and this showed clear ZnO peaks at 400 °C, which corresponded to the planes (100), (002), and (101). The PAN peak at 17° in Figure 4(b) became sharper with enhanced intensity because of its increased crystallinity. In the case of ZIF-8, Du *et al.*[39] reported similar results at 300 °C and above for long annealing times of more than 1 h.

The thermal stabilities of the pristine PAN NFs, ZIF-7/PAN NFs, and ZIF-7 NPs synthesized by the solvothermal method under atmospheric air are presented in Figure 5. In the case of the ZIF-7/PAN NFs, two important weight loss regions were identified between 25 and 800 °C. Approximately 40% of the weight loss was observed between 25 and 375 °C; this resulted from the removal of guest solvents, such as H_2O, methanol, and DMF.[36] This increased the porosity of the ZIF-7/PAN NFs. The second important weight loss of about 54.8% was observed

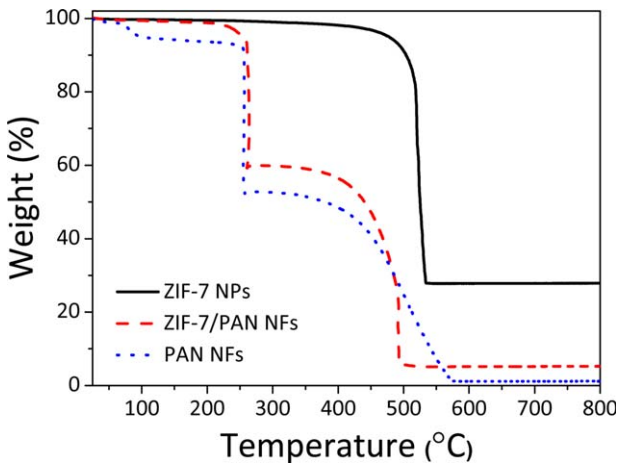

Figure 5. TGA of the ZIF-7 NPs and ZIF-7/PAN NFs under an air atmosphere. [Color figure can be viewed in the online issue, which is available at wileyonlinelibrary.com.]

between 400 and 500 °C and reflected the thermal decomposition of the structural framework of the ZIF-7/PAN NFs, which was associated with the decomposition of the organic linkers. This was accompanied by the formation of ZnO. Thus, TGA proved that the fabricated ZIF-7/PAN NFs were thermally stable up to about 400 °C; this was consistent with the XRD results presented previously. Furthermore, the chemical composition of the ZIF-7 NPs in the NFs was deduced by a comparison of the amount of remaining ZnO (>600 °C) of these NPs with that of the NFs. Our analysis found that about 27.8 wt % ZnO remained in the NPs and about 4.1 wt % ZnO was retained in the NFs (calculated by the subtraction of 1.1 wt % PAN from 5.2 wt % ZIF-7/PAN). That is, we determined that about 14.7% ZIF-7 NPs were initially embedded in the ZIF-7/PAN NFs. The estimated ZIF-7 loading value was in good agreement with the composition ratio used in the initial synthesis process.

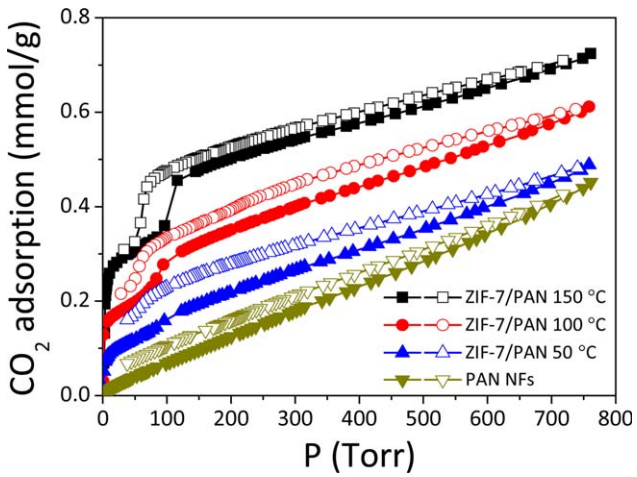

Figure 6. Adsorption/desorption isotherms of CO_2 (at 196 K) on ZIF-7/PAN NFs synthesized at 50, 100, and 150 °C. Closed symbols represent adsorption, and open symbols represent desorption. All samples were evacuated at 150 °C for 3 h before the sorption studies to remove entrapped solvents and moisture. P = pressure. [Color figure can be viewed in the online issue, which is available at wileyonlinelibrary.com.]

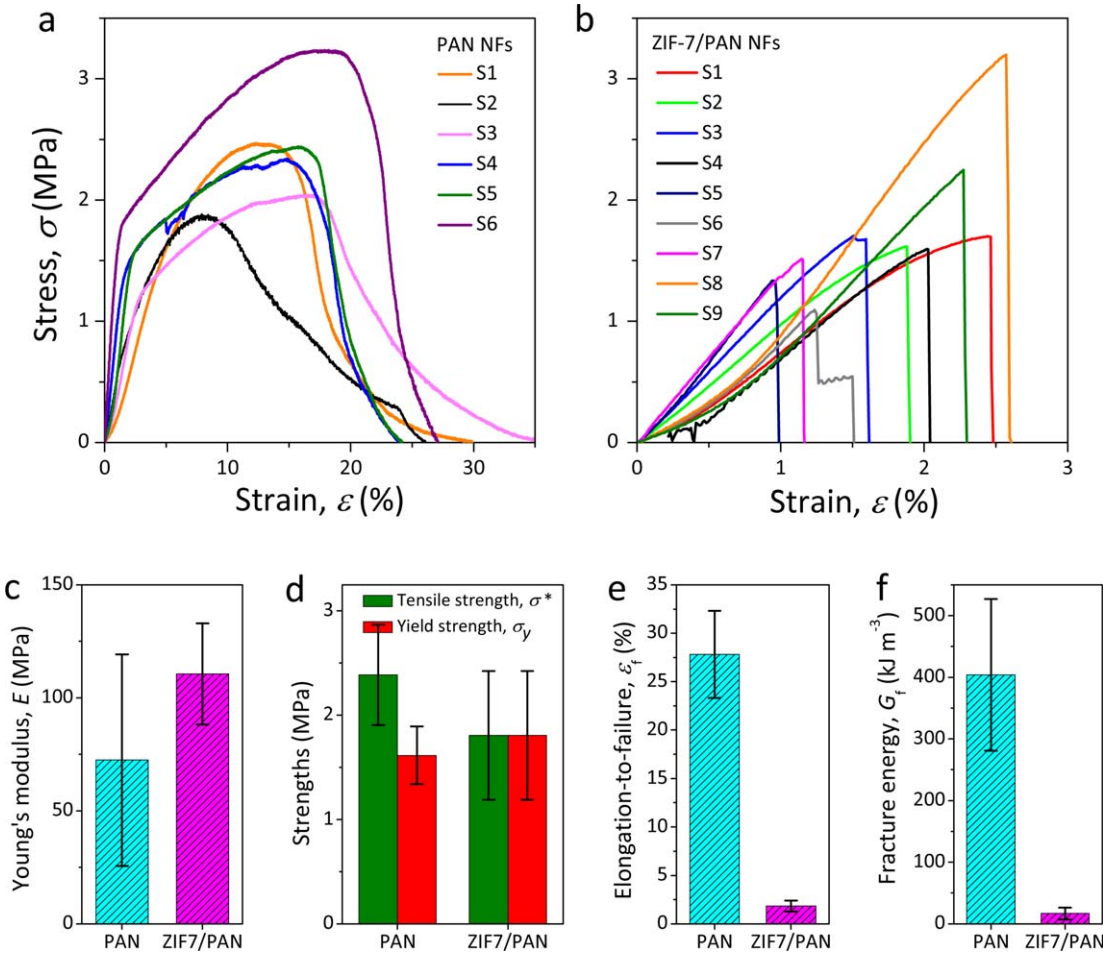

Figure 7. Nominal stress–strain curves measured under uniaxial tension for the (a) PAN and (b) ZIF-7/PAN NF mats. The mechanical properties derived from the nominal stress–strain curves include the following: (c) Young's modulus (E), which is a measure of the material stiffness (here determined from the gradient in the linear elastic region, which corresponded to strains of <1–2%); (d) yield strength (σ_y), which designates the level of stress after deviations from linearity start to develop and thus indicates the initiation of (irreversible) plastic deformation, and tensile strength (σ^*), which marks the maximum nominal stress level; (e) ε_f, which signifies the ductility or stretchability of the fiber material right up to the point of fracture (breakage); and (f) fracture energy per unit volume (G_f), which is a measure of the toughness and corresponds to the damage tolerance of the material (it is calculated by the integration of the area encompassed by the stress–strain curves from 0 to ε_f). [Color figure can be viewed in the online issue, which is available at wileyonlinelibrary.com.]

The hysteresis of the adsorption/desorption isotherms of CO_2 on the ZIF-7/PAN NFs synthesized at different synthesis temperatures are presented in Figure 6. Increasing the synthesis temperature was supposed to affect the formation of ZIF; this was hereby confirmed via the CO_2 adsorption results. With an increasing synthesis temperature, the formation of ZIF-7 was promoted (as explained in the XRD analysis; see Figure 4); this resulted in a markedly higher CO_2 adsorption capacity. Even though 50 °C was sufficient to crystallize ZIF-7, as evidenced by the solvothermal synthesis of the NPs, we established that 50 °C was not adequate to fully develop ZIF-7 in the NFs because the crystallization process was likely to be suppressed by the PAN polymer [Figure 1(a)]. However, it was not possible to increase the temperature above 150 °C because DMF contained in the ZIF-7/PAN solution evaporated at higher temperatures during the synthesis process. As observed in Figure 6, the ZIF-7/PAN NFs exhibited a stepwise CO_2 adsorption behavior at about 100 Torr (196 K) because of the transformation of narrow pores in the ZIF-7 structure to a larger pore configuration (gate-opening effect[11] after the stimulus of CO_2. These results were in good agreement with experimental data of van den Bergh *et al.*[35] determined at 195 K. On the contrary, there was no step change in the CO_2 adsorption for the neat PAN NFs (without ZIF-7). It is important to note that the magnitude of the stepwise increase in the CO_2 uptake of the ZIF-7/PAN NFs became more prominent with increasing synthesis temperature, that is, 150 > 100 > 50 °C. This finding supports the notion that the lesser adsorption of CO_2 was due to the underdeveloped ZIF-7 phase formed at a relatively lower synthesis temperature (in the presence of PAN). The measured CO_2 adsorptions in the cases where the syntheses were performed at 150, 100, and 50 °C at 760 Torr were about 0.72, 0.61, and 0.49 mmol/g, respectively, whereas about 4.9 mmol/g of CO_2 adsorption was observed in case of the ZIF-7 NPs (Supporting Information, Figure S1). The

comparative study of CO_2 adsorption on the ZIF-7 NPs and ZIF-7/PAN NFs showed that about 10–15 wt % ZIF-7 NPs was present on the NFs as the result of the one-step synthesis process. This was consistent with the TGA results. We anticipate that the CO_2 adsorption capacity could be enhanced further by higher loadings of ZIF-7 NPs onto the fibers. The full desorption curves of CO_2 in the ZIF-7/PAN NFs demonstrated the reusability of NF mats in reversible CO_2 capture or separation applications.

We conducted large-strain uniaxial tensile deformation experiments on the NF mats with and without ZIF-7 to establish the mechanical properties up to the point of material failure [elongation at failure (ϵ_f)]. Figure 7(a,b) presents the nominal stress–strain data recorded from a representative number of individual test specimens; this illustrated the material variability when the sample was subjected to mechanical loading on the basis of the stochastic nature of the fiber architecture and its distribution. Noticeably, there was a considerable amount of plastic deformation accompanied by strain hardening when the mat was stretched beyond the elastic limit ($\epsilon_f \approx$ 1–2%); this translated into a high ductility value of about 28% before fracture. On the contrary, plastic deformation was suppressed after the inclusion of the ZIF-7 NPs into the PAN matrix; this caused the ductility to decline substantially by one order of magnitude and approach a level of about 2%. It was clear that the mechanical deformation of the ZIF-7/PAN NFs could be considered to be brittle in nature (small ϵ_f), and rupture occurred more abruptly beyond the tensile strength (σ^*). Such a ductile-to-brittle transition could be associated with the disrupted and discontinuous microstructure evidenced in the TEM images of the NFs (Figure 2), as opposed to the pure PAN fibers. With respect to the Young's modulus and strength properties [Figure 7(c,d)], however, we found that the differences between the neat PAN and ZIF-7/PAN NF mats were, in fact, small and could be accounted for by the relatively large error margins. However, the reduced ductility [Figure 7(e)] implied that the corresponding fracture energy [toughness; Figure 7(f)] was also affected; in practice, this might not have posed a significant hindrance if the electrospun mats could be supported (e.g., encased or sandwiched) by means of a more robust substrate. Of course, another practicable strategy is to engineer the thin electrospun nanocomposite mats (~10 s μm) to generate thicker laminated NF mats (e.g., ~100 s μm to ~1 mm in thickness, without permeability degradation), whose damage tolerance and mechanical stability would be enhanced.

CONCLUSIONS

In summary, we have developed a one-step process for the fabrication of ZIF-7/PAN NFs by electrospinning for the first time. The XRD characterization confirmed the formation of ZIF-7 in the NFs, and these composite NFs, with the average diameter of 245 nm, showed markedly improved CO_2 adsorption and desorption characteristics. This makes them attractive for gas separation and other selective filtration applications. The CO_2 adsorption capacity can potentially be tuned or enhanced through the control of the weight percentage loading of the ZIF-7 NPs embedded in the fiber. The proposed methodology of the ZIF-7/PAN NF fabrication is also scalable; this will enable the production of large-size mats that are desirable for practical applications. The freestanding electrospun mats demonstrated reasonably good handleability, mechanical resilience, and damage tolerance, and this will pave the way for many useful industrial applications.

ACKNOWLEDGMENTS

This work was supported by the Industrial Strategic Technology Development Program (contract grant number 10045221), which is funded by the Korean Ministry of Knowledge Economy (contract grant numbers NRF-2013M3A6B1078879 and NRF-2013R1A2A2A05005589). The authors extend their appreciation to the Deanship of Scientific Research at King Saud University for its funding of this prolific research group (contract grant number PRG-1436-03). One of the authors (Y.K.H.) is grateful for financial support from the Agency for Defense Development of Korea (contract grant number UC1400261D).

REFERENCES

1. Li, J.-R.; Ma, Y.; McCarthy, M. C.; Sculley, J.; Yu, J.; Jeong, H.-K.; Balbuena, P. B.; Zhou, H.-C. *Coord. Chem. Rev.* **2011**, *255*, 1791.
2. Drage, T. C.; Snape, C. E.; Stevens, L. A.; Wood, J.; Wang, J.; Cooper, A. I.; Dawson, R.; Guo, X.; Satterley, C.; Irons, R. *J. Mater. Chem.* **2012**, *22*, 2815.
3. Davison, J.; Thambimuthu, K. *Proc. Inst. Mech. Eng. Part A* **2009**, *223*, 201.
4. Yu, C.-H.; Huang, C.-H.; Tan, C.-S. *Aerosol Air Qual. Res.* **2012**, *12*, 745.
5. Sumida, K.; Rogow, D. L.; Mason, J. A.; McDonald, T. M.; Bloch, E. D.; Herm, Z. R.; Bae, T.-H.; Long, J. R. *Chem. Rev.* **2011**, *112*, 724.
6. Chaemchuen, S.; Zhou, K.; Kabir, N. A.; #Chen, Y.; Ke, X.; Van Tendeloo, G.; Verpoort, F. *Micropor. Mesopor. Mater.* **2015**, *201*, 277.
7. Hwang, Y. K.; Hong, D. Y.; Chang, J. S.; Jhung, S. H.; Seo, Y. K.; Kim, J.; Vimont, A.; Daturi, M.; Serre, C.; Férey, G. *Angew. Chem. Int. Ed.* **2008**, *47*, 4144.
8. Horcajada, P.; Chalati, T.; Serre, C.; Gillet, B.; Sebrie, C.; Baati, T.; Eubank, J. F.; Heurtaux, D.; Clayette, P.; Kreuz, C. *Nat. Mater.* **2010**, *9*, 172.
9. Park, K. S.; Ni, Z.; Côté, A. P.; Choi, J. Y.; Huang, R.; Uribe-Romo, F. J.; Chae, H. K.; O'Keeffe, M.; Yaghi, O. M. *Proc. Natl. Acad. Sci.* **2006**, *103*, 10186.
10. Tan, J. C.; Bennett, T. D.; Cheetham, A. K. *Proc. Natl. Acad. Sci.* **2010**, *107*, 9938.
11. Ryder, M. R.; Civalleri, B.; Bennett, T. D.; Henke, S.; Rudić, S.; Cinque, G.; Fernandez-Alonso, F.; Tan, J.-C. *Phys. Rev. Lett.* **2014**, *113*, 215502.
12. Liu, S.; Xiang, Z.; Hu, Z.; Zheng, X.; Cao, D. J. *Mater. Chem.* **2011**, *21*, 6649.
13. Lu, G.; Li, S.; Guo, Z.; Farha, O. K.; Hauser, B. G.; Qi, X.; Wang, Y.; Wang, X.; Han, S.; Liu, X. *Nat. Chem.* **2012**, *4*, 310.

14. Zhu, M.; Srinivas, D.; Bhogeswararao, S.; Ratnasamy, P.; Carreon, M. A. *Catal. Commun.* **2013**, *32*, 36.
15. Yue, Y.; Mehio, N.; Binder, A. J.; Dai, S. *CrystEngComm* **2015**, *17*, 1728.
16. Liang, K.; Ricco, R.; Doherty, C. M.; Styles, M. J.; Bell, S.; Kirby, N.; Mudie, S.; Haylock, D.; Hill, A. J.; Doonan, C. J. *Nat. Commun.* **2015**, *6*, 7240.
17. Cai, W.; Lee, T.; Lee, M.; Cho, W.; Han, D.-Y.; Choi, N.; Yip, A. C. K.; Choi, J. *J. Am. Chem. Soc.* **2014**, *136*, 7961.
18. Yao, J.; Wang, H. *Chem. Soc. Rev.* **2014**, *43*, 4470.
19. Breck, D. W. Zeolite Molecular Sieves: Structure, Chemistry and Use; Wiley: New York, **1974**.
20. Gücüyener, C.; van den Bergh, J.; Gascon, J.; Kapteijn, F. *J. Am. Chem. Soc.* **2010**, *132*, 17704.
21. Li, Y.; Liang, F.; Bux, H.; Yang, W.; Caro, J. J. *Membr. Sci.* **2010**, *354*, 48.
22. Fan, L.; Xue, M.; Kang, Z.; Li, H.; Qiu, S. J. *Mater. Chem.* **2012**, *22*, 25272.
23. Tanh Jeazet, H. B.; Staudt, C.; Janiak, C. *Dalton Trans.* **2012**, *41*, 14003.
24. Ostermann, R.; Cravillon, J.; Weidmann, C.; Wiebcke, M.; Smarsly, B. M. *Chem. Commun.* **2011**, *47*, 442.
25. Lange, L.; Ochanda, F.; Obendorf, S. K.; Hinestroza, J. *Fibers Polym.* **2014**, *15*, 200.
26. Kang, C.-H.; Lin, Y.-F.; Huang, Y.-S.; Tung, K.-L.; Chang, K.-S.; Chen, J.-T.; Hung, W.-S.; Lee, K.-R.; Lai, J.-Y. J. *Membr. Sci.* **2013**, *438*, 105.
27. Zhang, W.; Wu, Z.-Y.; Jiang, H.-L.; Yu, S.-H. *J. Am. Chem. Soc.* **2014**, *136*, 14385.
28. Wu, B.; Pan, J.; Ge, L.; Wu, L.; Wang, H.; Xu, T. *Sci. Rep.* **2014**, *4*, 1.
29. Biswal, B. P.; Bhaskar, A.; Banerjee, R.; Kharul, U. K. *Nanoscale* **2015**, *7*, 7291.
30. Bechelany, M.; Drobek, M.; Vallicari, C.; Chaaya, A. A.; Julbe, A.; Miele, P. *Nanoscale* **2015**, *7*, 5794.
31. Huang, X.; Zhang, J.; Chen, X. *Chin. Sci. Bull.* **2003**, *48*, 1531.
32. Lu, G.; Farha, O. K.; Zhang, W.; Huo, F.; Hupp, J. T. *Adv. Mater.* **2012**, *24*, 3970.
33. Stassen, I.; Styles, M.; Grenci, G.; Van Gorp, H.; Vanderlinden, W.; De Feyter, S.; Falcaro, P.; De Vos, D.; Vereecken, P.; Ameloot, R. *Nat. Mater.* **2015**, *15*, 304.
34. Tan, J. C.; Cheetham, A. K. *Chem. Soc. Rev.* **2011**, *40*, 1059.
35. van den Bergh, J.; Gücüyener, C.; Pidko, E. A.; Hensen, E. J. M.; Gascon, J.; Kapteijn, F. *Chem.–Eur. J.* **2011**, *17*, 8832.
36. Li, F.; Bao, X. X.; Yu, X. F. *Korean Chem. Eng. Res.* **2014**, *52*, 340.
37. Ma, G.; Yang, D.; Nie, J. *Polym. Adv. Technol.* **2009**, *20*, 147.
38. Bennett, T. D.; Keen, D. A.; Tan, J. C.; Barney, E. R.; Goodwin, A. L.; Cheetham, A. K. *Angew. Chem.* **2011**, *123*, 3123.
39. Du, Y.; Chen, R. Z.; Yao, J. F.; Wang, H. T. *J. Alloys Compd.* **2013**, *551*, 125.

SGML and CITI Use Only
DO NOT PRINT